2025.

Detecting causality in the frequency domain with Cross-Mapping Coherence [1].

Understanding causal relationships within a system is crucial for uncovering its underlying mechanisms. Causal discovery methods, which facilitate the construction of such models from time series data, hold the potential to significantly advance scientific and engineering fields.

We introduced the Cross-Mapping Coherence (CMC) method, designed to reveal causal connections in the frequency domain between time series. CMC builds upon nonlinear state-space reconstruction and extends the Convergent Cross-Mapping algorithm to the frequency domain by utilizing coherence metrics for evaluation. We tested the CMC method using simulations of logistic maps, Lorenz systems, Kuramoto oscillators, and the Wilson–Cowan model of the visual cortex. CMC accurately identified the direction of causal connections in these simulated scenarios. When applied to the Wilson–Cowan model, CMC was able to disentangle feedforward alpha and feedback gamma coupling between the V1 and V4 areas, supporting the results of previous analysis.

Furthermore, CMC could detect weak connections (), demonstrated sample efficiency (), and maintained robustness in the presence of noise up to on unidirectionally coupled logistic map systems. In conclusion, the capability to determine directed causal influences across different frequency bands allows CMC to provide valuable insights into the dynamics of complex, nonlinear systems.

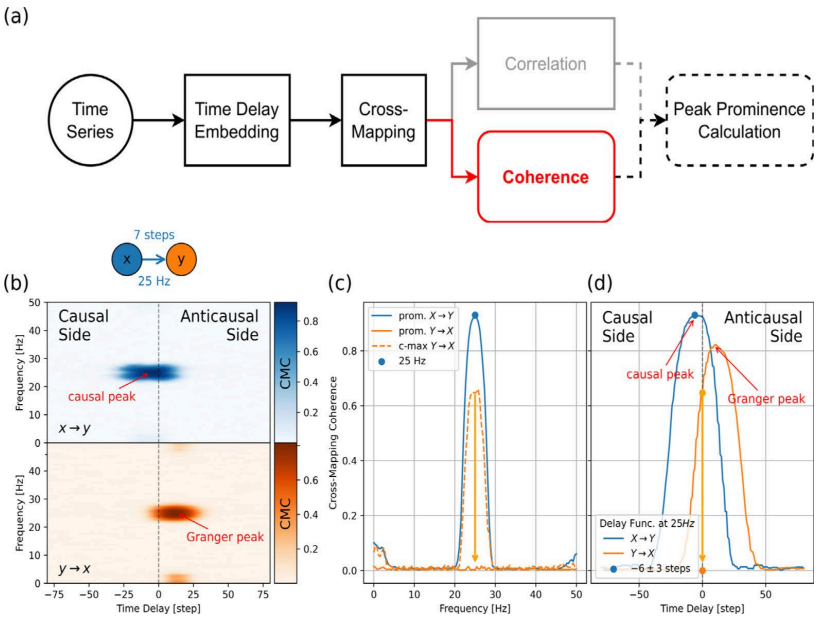

Figure 2. Cross-Mapping Coherence (CMC) detects causal relationships in the frequency domain and filters out spurious connections via peak prominence calculation. (a) Workflow Overview: Two time series undergo time-delay embedding, followed by cross-mapping to generate predictions at various time delays. A coherence-based evaluation refined by peak-prominence calculation quantifies the causal interactions across frequencies, providing spectral insight into the relationship. **(b)–(d)** Illustrative Example: CMC output for unidirectionally coupled logistic maps x and y. The subsystems are linearly coupled around the 25 ± 1.5 Hz frequency band, 7-step coupling delay, ε = 0.4 coupling strength, and n = 50 k time series length. (E = 5, τ = 1step) (b) Frequency-Delay Representation: The CMC function is shown for both directions ($x \rightarrow y$ and $y \rightarrow x$), with the causal side (negative delays) and anticausal side (positive delays) indicated. Stronger colors correspond to higher coherence, highlighting causal interactions at specific frequencies and delays. **(c)** Frequency Representation: Prominence values over frequency bands are computed by identifying and measuring the most prominent peaks on the causal side of the CMC function along the time-delay axis. If no peak is detected on the causal side for a given frequency, the prominence is set to zero. This approach ensures that only meaningful causal

effects are considered, while filtering out spurious influences, such as Granger peaks on the anticausal side. In contrast, the maximum of the CMC function on the causal side (dashed curve) indicates spurious connections. **(d)** CMC at 25 Hz: The CMC function at the identified peak frequency (25 Hz) illustrates how peaks on the causal side are selected to determine causal influence. These values form the basis of the causal inference in (c), providing a refined and frequency-specific measure of causal connections.

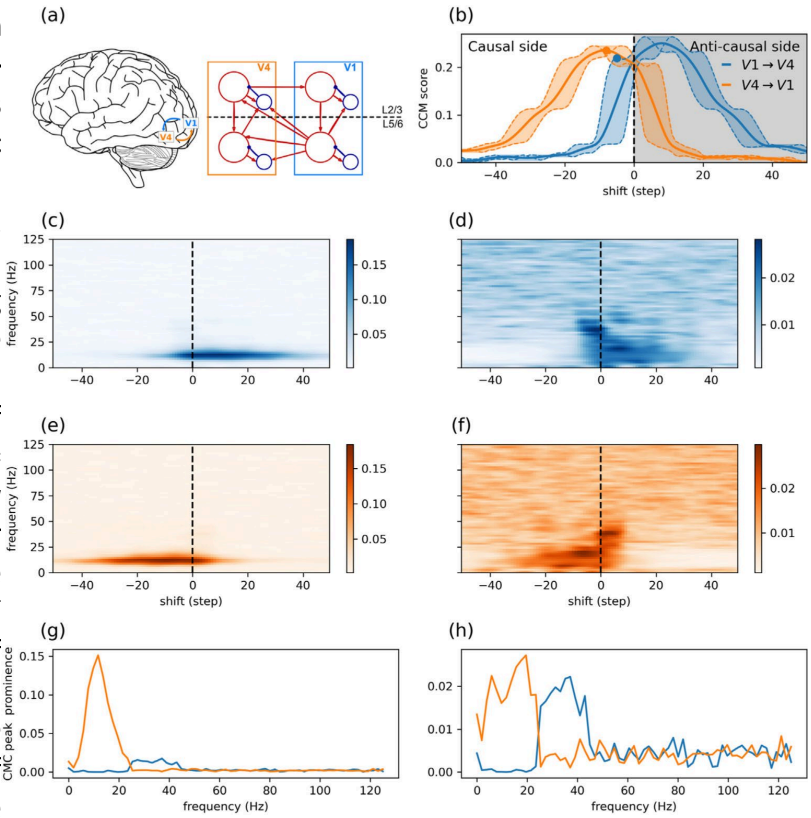

Figure 2. Causal discovery with CCM and CMC on a Wilson–Cowan model of cortical areas V1 and V4. (a) Schematic illustration of the network. Each area is modeled by 2 × 2 stochastic differential equations. The coupling strengths are chosen to be biologically appropriate. **(b)** Time-delayed CCM analysis of the Wilson–Cowan dataset (E = 9, τ = 1). The solid curves show the average performance over reconstructed state coordinates and realizations (N = 10) in the function of temporal shift, whereas dashed lines denotes the score for the first and the last coordinates of the embeddings, with the transition between these latter two marked as shading giving a sense about the temporal uncertainty of effect propagation delay. The V 4 → V 1 connection is stronger at the −8 timesteps shift (orange). **(c, e)** Shift-frequency CMC analysis shows a strong peak at the 5−20 Hz range for the V 4 → V 1 connection on (e) and the corresponding Granger-peak on the anti-causal side on **(c)**. **(d, f)** The same peak is present on the band-normalized CMC functions on **(f)**, but an additional peak becomes visible in the opposite direction (V 1 → V 4) at the 20−50 Hz range on **(d)**. **(g, h)** CMC prominence reveals frequency-specific causal interactions between V1 and V4, both for the raw **(g)** and the normalized **(h)** case. From V1 to V4, the causal effect appears in the 20−50 Hz range, whereas the V4 to V1 coupling takes shape in the 1−20 Hz frequency band.

References:

[1] https://doi.org/10.1016/j.physd.2025.134708

[2] https://doi.org/10.1002/sres.70003

[3] https://doi.org/10.48550/arXiv.2410.19469

[4] https://doi.org/10.1016/j.neunet.2025.108113

[5] https://doi.org/10.1101/2025.04.11.648355